Article:
Zhai, X, Zou, X, Shi, J et al. (10 more authors) (2020) Amine-responsive bilayer films with improved illumination stability and electrochemical writing property for visual monitoring of meat spoilage. Sensors and Actuators, B: Chemical, 302. 127130. ISSN 0925-4005

https://doi.org/10.1016/j.snb.2019.127130

Amine-responsive bilayer films with improved illumination stability and electrochemical writing property for visual monitoring of meat spoilage

Xiaodong Zhai [a], Xiaobo Zou [a,*], Jiyong Shi [a,*], Xiaowei Huang [a], Zongbao Sun [a], Zhihua Li [a], Yue Sun [a], Yanxiao Li [a], Xin Wang [a], Melvin Holmes [b], Yunyun Gong [b], Megan Povey [b], Jianbo Xiao [c]

[a] Agricultural Product Processing and Storage Lab, School of Food and Biological Engineering, Jiangsu University, Zhenjiang, Jiangsu 212013, China

[b] School of Food Science and Nutrition, University of Leeds, Leeds LS2 9JT, United Kingdom

[c] Institute of Chinese Medical Sciences, State Key Laboratory of Quality Research in Chinese Medicine, University of Macau, Taipa, Macau, China

*Corresponding author. Tel.: +86 511 88780174; Fax: +86 511 88780201; Email: zou_xiaobo@ujs.edu.cn (Xiaobo Zou), Shi_jiyong@ujs.edu.cn (Jiyong Shi).

Abstract

Amine-responsive bilayer films were developed by using agar (AG), anthocyanins (AN), gellan gum (GG) and TiO_2 nanoparticles for visual monitoring of meat spoilage. The AG-AN layer worked as the sensing layer to volatile amines, while GG-TiO_2 layer served as the light barrier layer and simultaneously the conducting layer to improve the illumination stability and electrochemical writing ability of the AG-AN layer, respectively. The Scanning electron microscopy (SEM) images and X-ray diffraction (XRD) spectra indicated the successful fabrication of bilayer films. Illumination experiments showed that the incorporation of TiO_2 in the GG-TiO_2 layer significantly improved the illumination stability of AN in the AG-AN layer. Meanwhile, electrochemical writing process could be easily conducted on the AG-AN layer in the presence of GG-TiO_2 layer, indicating the feasibility of ink-free printing on bilayer biopolymer films. The AG-AN/GG-2%TiO_2 film presented a limit of detection of 0.018 mM to trimethylamine (TMA), a typical basic gas generated during meat spoilage. Based on its good illumination stability and sensing ability to basic gases, the AG-AN/GG-2%TiO_2 film exhibited rose red-to-green color changes along with the spoilage of pork and silver carp, indicating its great potential for monitoring meat spoilage in intelligent food packaging.

Keywords

Bilayer films, anthocyanins, electrochemical writing, amines, meat, intelligent packaging

1. Introduction

Meat spoilage during distribution can be considered as an ecological phenomenon. Unfortunately, meat spoilage could cause not only food waste, but more serious food safety issues, because most of the specific spoilage organisms [1] and their metabolites are harmful to human body. From the perspective of food preservation and food safety assurance, it is of great significance to detect the meat spoilage in supply chain. To date, in most cases, the meat spoilage was determined by using destructive detection methods, such as the determination of total volatile base nitrogen (TVB-N) and total viable count (TVC). However, it is always a tedious work to determine the meat spoilage, especially when the number of samples is very large. Hence, it is highly desirable to develop simple, cost-effective and non-destructive sensing technologies for the rapid detection of real-time meat spoilage.

Intelligent food packaging has received considerable attention in modern food industry. It especially aims to monitor the food quality or the surrounding environment of foods by using sensors, indicators, and data carriers, which goes beyond the traditional food packaging mainly with barrier abilities. These sensors, indicators and data carriers are equipped onto or into the packages so that they can in situ record the information of food quality. Among various sensors in intelligent packaging, colorimetric sensors, such as thin films [2, 3], hydrogels [4-8] and colorimetric arrays [9], have attracted much attention because they are portable, easy to fabricate and convenient for visual detection.

In recent years, various pH-sensitive colorimetric films have been developed as the gas sensors to monitor the meat spoilage. These pH-sensitive colorimetric films could exhibit visible color changes when reacting with the non-neutral volatile gases, such as amines [10] and carbon dioxide [11], generated from deteriorated meats. Considering that traditional synthetic pH dyes had potential harmful effects on human beings, of late, much attention has been paid to natural pH-responsive pigments, such as anthocyanins [7, 12-24] and curcumin [25-28], which are safe and edible. At the same time, biopolymers, including polysaccharides and proteins, were employed to immobilize these natural pigments due to their good compatibility with natural pigments. However, one of the major concerns of these anthocyanins-polymer blend films would be the intrinsic instability of anthocyanins

against ultraviolet (UV) light, temperature and oxygen [29]. Among these factors, UV light irradiation should be a key factor to the color stability of anthocyanins embedded into biopolymer films in practical application. This is because the meat packaging could inevitably be exposed to sunlight in the supply chain. In addition, some studies showed that the UV light had a higher impact on anthocyanin stability than elevated temperatures [30, 31]. Hence, it is critical to improve the light resistance ability of anthocyanins-based films to achieve a long-term color stability.

Printing on food packaging materials can provide important information about foods, such as the manufacture date and storage status of foods [32]. However, most inks are typically derived from petrochemical feedstock, which brings not only environmental sustainability concerns, but also food safety risk due to the possible migration of inks from the package surface to foods. In recent years, the electrochemical writing technology has emerged for printing on biopolymer films [32, 33]. Our previous study showed that colorful patterns could be printed on the anthocyanins-polymers blend films based on the pH-responsive color change of anthocyanins [34]. By using anthocyanins as the color agent, this electrochemical writing can be regarded as a green printing method.

Hence, in this study, we aimed to develop a bilayer film with improved illumination stability and electrochemical writing ability to monitor meat spoilage. The first layer of the bilayer film is agar-anthocyanins (AG-AN) blend, working as the sensing layer. The anthocyanins were extracted from rose (Rosa rugosa), which are readily available at low cost. Agar is an edible polysaccharide with good film-forming ability, and the use of the agar to immobilize the anthocyanins was due to its near neutral charge that had no interference to the color change of anthocyanins. The second layer of the bilayer film is the gellan gum-titanium dioxide (GG-TiO_2) blend, which was employed as the protection layer. It is well known that rutile TiO_2 nanoparticles had excellent UV-blocking power by absorbing high-energy UV and transforming them into less harmful heat or fluorescence [35]. Hence, rutile TiO_2 nanoparticles was used to improve the illumination stability of anthocyanins by protecting the anthocyanins in the sensing layer from UV irradiation. GG is also a natural edible polysaccharide with good film-forming ability. A previous study showed that GG was a good polymer matrix to support and immobilize TiO_2 nanoparticles

[36]. Therefore, TiO_2 nanoparticles were embedded in the GG matrix to reduce aggregation. At the same time, with the help of GG-TiO_2 composite as a conducting layer, electrochemical writing could be easily conducted on the AG-AN layer. To our best knowledge, this is the first study trying to develop bilayer films with improved illumination stability of anthocyanins and electrochemical writing performance. Our study showed that the fabricated bilayer colorimetric films were sensitive to volatile amines. The addition of rutile TiO_2 nanoparticles improved the illumination stability of the embedded anthocyanins, and multicolor patterns could be printed on AG-AN layer by using the electrochemical writing method. The bilayer colorimetric film, working as a gas sensor, exhibited visible color changes along with the spoilage of pork and fish samples, indicating their good potential in visual monitoring of meat spoilage in intelligent packaging.

2. Materials and methods

2.1. Materials and Reagents

Dried rose (Rosa rugosa), fresh pork and live silver carp (Hypophthalmichthys molitrix) were purchased from local market (Zhenjiang, China). Low-acyl gellan gum was bought from Dancheng Caixin sugar industry Co., ltd. (Dancheng, China). Rutile titanium dioxide nanoparticles (diameter ~60 nm) was bought from Rhawn Chemicals. Agar, ethanol, calcium chloride and trimethylamine solution (33 wt%) were bought from Sinopharm Chemical Reagent Co., Ltd (Shanghai, China).

2.2. Anthocyanins extraction

Dried roseleaf was crushed into powder and transferred to 80% ethanol aqueous solution with a solid-liquid ratio of 1:15. This mixture was stirred at 35 °C for 6 h and then was filtrated using a 25-μm filter paper to collect the supernatant. Ethanol in the supernatant was removed with a vacuum rotary evaporator at 45 °C in dark. The concentrated anthocyanins extract solution was freeze-dried to obtain anthocyanins extract powders, which were stored at 4 °C in a brown bottle filled with nitrogen.

The anthocyanins content in the extract powder was measured by the pH differential method [37] and anthocyanins content was expressed in mg/g (anthocyanins/extract powder).

2.3. Preparation of bilayer films

The bilayer films were prepared by a two-step casting method. A quantity of 2 g of AG powder was added to 100 mL of water and the mixture was heated at 98 ℃ under stirring for 2 h to form a clear solution. When the AG solution was cooled to 45 ℃, a certain amount of lyophilized AN powder was added to the AG solution to obtain an AN content of 8 mg/100 mL, according to the AN content in the lyophilized AN extract powder (612 mg/g) (refer to section 2.2). After degassed with a sonicator (Branson CPX5800H, USA), the solution (6 mL) was immediately poured into a smooth plastic Petri dish (diameter 53 mm) on a horizontal table. Firm AG-AN hydrogel was formed when the AG-AN solution was cooled.

Meanwhile, a quantity of 2 g of GG powder was dissolved in 100 mL of water by heating at 80 ℃ under stirring. TiO_2 nanoparticles powders in ratio of 0.5, 1.0 and 2.0 g/100 g of GG were firstly dispersed in 2 mL of water and then sonicated for 5 min. Then, the TiO_2 dispersion was dropwise added to the GG solution with continuous stirring. Under this temperature, the mixtures were sonicated with a sonicator for 10 min, and subsequently stirred for 10 min. After that, 5 mL of $CaCl_2 \cdot 2H_2O$ solution (8 mg/mL) was dropwise added into the solution with continuous stirring. When the GG- GG-TiO_2 solution was cooled down to 50 ℃, 6 mL of the solution was immediately poured on the as-prepared AG-AN hydrogel. After the solutions was cooled, firm GG-TiO_2 hydrogels were formed on the upper surface of the AG-AN hydrogel. The GG hydrogels containing TiO_2 in the concentration of 0, 0.5, 1.0 and 2.0 g/100 g of GG were expressed as GG, GG-0.5%TiO_2, GG-1%TiO_2 and GG-2%TiO_2 hydrogel, respectively.

The as-prepared bilayer hydrogels were dried to films at 50 ℃ under vacuum, and the obtained films were peeled from the Petri dish and stored at 4 ℃ with 75% relative humidity (RH) for further use. The bilayer films containing AG-AN and GG with different contents of TiO_2 were expressed as AG-AN/GG, AG-AN/GG-0.5%TiO_2, AG-AN/GG-1%TiO_2, and AG-AN/GG-2%TiO_2 films, respectively. In addition, the bilayer film without AN and TiO_2 was also prepared and expressed as AG/GG film. The preparation process of bilayer films were described in **Scheme 1**.

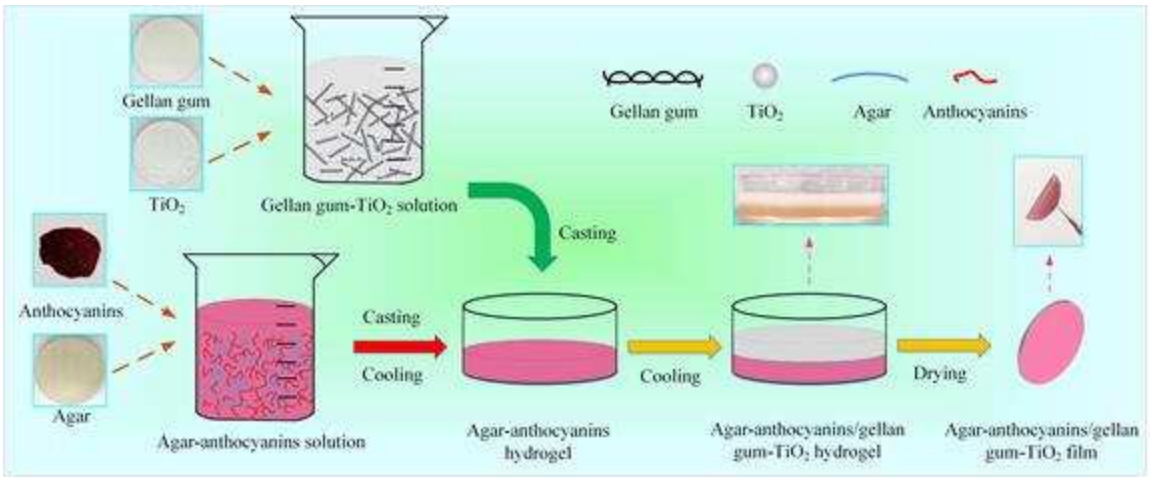

Scheme 1. The two-step casting process of fabricating the bilayer colorimetric films.

2.4. Electrochemical writing on bilayer films

The electrochemical writing on the films were conducted following the procedure in our previous study with a slight modification [34]. The above mentioned bilayer hydrogels were firstly taken out from the Petri dish before drying. The bottom layer (GG-TiO_2) hydrogel was completely put on a platinum (Pt) plate (60 × 60 × 0.2 mm), and the upper layer (AG-AN) hydrogel was connected with the Pt needle (diameter 0.5 mm). The Pt plate and Pt needle were respectively connected with the cathode and anode of an electrochemical analyzer (CHI660E, CH Instruments Co., Shanghai, China). The movement of the Pt needle was procedurally controlled by a robotic arm (DOBOT M1, Shenzhen Yuejiang Technology Co., Ltd, China), with a step precision of 0.1 μm. The bilayer hydrogels were immediately dried in a vacuum-drying oven at 70 °C to form thin bilayer films after the electrochemical writing process, and the films were also stored at 4 °C with 75% RH before use.

2.5. Characterization of the films

2.5.1. Microstructure observation

The micrographs of the films were recorded by a field emission scanning electron microscopy (FE-SEM) (S-4800, Hitachi High Technologies Corporation, Japan). The films were freeze fractured by liquid nitrogen for cross section observation. Then, they were attached to conductive adhesive tape and mounted on the specimen holder, and finally

coated with gold under vacuum. TiO_2 nanoparticles were dispersed on silicon wafer for SEM observation and energy dispersive X-ray spectroscopy (EDS) analysis.

2.5.2. X-ray diffraction spectra

X-ray diffraction (XRD) spectra of TiO_2 nanoparticles and the films were measured using an X-ray diffractometer (D8 ADVANCE, Bruker, Germany) equipped with monochromatic Cu-Kα radiation, under a voltage of 40 kV and a current of 40 mA. The samples were measured in continuous scan mode from 10 to 80° with a step of 2°/min.

2.5.3. Mechanical properties

The thickness of the films was firstly measured by using a hand-held digital micrometer (Sanfeng Group Co., Ltd., Taiwan, China). Tensile strength (TS) and elongation-at-break (EB) of the films were measured with a Model 4500 Universal Testing Machine (Instron Corporation, Canton, MA), using a modified American Standards for Testing and Materials (ASTM) standard procedure (ASTM Standard D882-00, 2000) procedure. Samples were conditioned in a desiccator containing saturated $Mg(NO_3)_2$ solution for 2 days prior to analysis. Each film was cut to a rectangular strip (30 × 20 mm). The grip separation and tensile speed were set at 20 mm and 0.6 mm/s respectively. TS and EB were calculated using eqs 1 and 2, respectively:

$$TS = \frac{F}{S} \quad (1)$$

$$EB(\%) = 100 \times \frac{\Delta l}{l_0} \quad (2)$$

where TS is the tensile strength; F is the maximum load; S was the initial cross-sectional area of the film sample; EB was the elongation at break; Δl is the extension of the films and l_0 is the initial test length of the films.

2.5.4. Water vapor permeability

The water vapor permeability (WVP) of the films was measured using the ASTM method (ASTM Standard E96M-05, 1995). A glass cup with silica gel was closed with a sample of film firmly fixed on top. The cups were weighed and placed in a desiccator

containing saturated $Mg(NO_3)_2$ solution, which provided an relative humidity of 50% at 25 °C. The cups were weighed every 4 h until a steady increase in weight was achieved. The water vapor transferred through the films and absorbed by the desiccant was determined from the weight gain of the cup. The water vapor transmission rate (WVTR) and WVP were calculated using eqs 3 and 4, respectively:

$$WVTR = \frac{\Delta m}{A \times \Delta t} \quad (3)$$

$$WVP = WVTR \times \frac{x}{\Delta p} \quad (4)$$

where $\Delta m/\Delta t$ is the amount of water gain per unit time of transfer; A is the area exposed to water transfer; x is the film thickness, and ΔP is the water vapor pressure difference between both sides of the film.

2.5.5. Oxygen permeability

The Oxygen permeability (OP) of the films was determined following the ASTM method (ASTM D3985-05, 2005) at 25 °C and 53% relative humidity. OP values were calculated by dividing oxygen transmission rate (OTR) by the numerical difference in partial oxygen pressure on both sides of the films and multiplying by the mean thickness of the films, using eq 5:

$$OP = OTR \times \frac{x}{\Delta P} \quad (5)$$

where x is the film thickness and ΔP is the partial pressure of oxygen. Measurements represent an average of six samples.

2.6. Color stability to light

The color stability of the films under visible light ($\lambda \approx$ 400-760 nm, 18 W, Philips, Netherlands) and UV light (λ = 320-400 nm with λ_{max} = 350 nm, 15 W, 40 uw/cm^2, Guanya Optoelectronic Technologies Co., Ltd) were investigated in a temperature controlled cabinet (25 °C). The lights irradiated the GG-TiO_2 layers for each film. The distance between the films and the light sources was 20 cm. The images of the films under visible

light and UV light were captured every 3 d and 5 h, respectively, using an optical scanner. The color parameters of the films were analyzed by using a user program in Matlab R2012a (Matworks Inc., Natick, MA, USA). To compare the color stability of the films with different initial colors, the relative color change (S) of the films were defined as eqs 6-9, according to our previous study [38]:

$$\Delta R = \left| R_0 - R_1 \right| \tag{6}$$

$$\Delta G = \left| G_0 - G_1 \right| \tag{7}$$

$$\Delta B = \left| B_0 - B_1 \right| \tag{8}$$

$$S(\%) = 100 \times \frac{\Delta R + \Delta G + \Delta B}{R_0 + G_0 + B_0} \tag{9}$$

where S is the relative color change of R, G and B values; R_0, G_0, B_0 are respectively the initial gray values of the red, green and blue of the film; R_1, G_1, B_1 are respectively the gray values of the red, green and blue of the film after storage.

2.7. Color response to trimethylamine

Trimethylamine (TMA) was used as the representatives of volatile basic gases generated from spoiled meats. The film strips (10×10 mm) were hung up in a testing chamber with the constant temperature (25°C) and relative humidity (75%). The solution of the analyte was injected into the testing chamber with a microliter syringe [23]. The concentration of TMA in the chamber was calculated using eq 10:

$$C = \frac{\rho_s V_s W}{M V} \tag{10}$$

Where C (mol/L) is the analyte concentration in the testing chamber; ρ_s is the density of analyte solution (g/mL); V_s is the volume of the liquid analyte (mL); W is the mass fraction of analyte in the solution; M is the molar mass of the analyte (g/mol); V is the volume of the testing chamber (L).

The films were maintained in the testing chamber for 3 h to reach reaction equilibrium. After that, the images and the UV-Vis spectra of the films were recorded using an optical scanner and the UV-Vis spectrophotometer, respectively.

2.8. Application of films in monitoring meat spoilage

Fresh pork was directly diced without further treatment. Live silver carp was also diced after removing its innards, head, tail and feathers. A quantity of 200 g of diced pork and silver carp were put into a polythylene terephthalate (PET) box with a buttoned lid. Two AG-AN/GG-2%TiO_2 films, of which the AG-AN layer faced downwards, were respectively fixed on the lid to cover the hole (15 × 15 mm) on the lid and adhered onto the internal surface of the PET lid. The PET box was placed in an incubator at 4 ℃ with 75% RH. The photos of the films used to monitor meat spoilage were obtained by using a digital camera, and the color parameters were extracted by using the Matlab software.

The total volatile basic nitrogen (TVB-N) content of these meat samples was measured according to a previous literature [39], following the Chinese Standard (GB 5009. 228-2016).

2.9. Statistical analysis

Duncan's multiple range test was used to compare the means at the 95% confidence level by using SPSS statistics software. The data labeled with different lowercase letters are significantly different.

3. Results and discussion

3.1. Characterization of the films

3.1.1. SEM images analysis

Fig. 1 shows the SEM images of cross sections of the films. A bilayer structure could be clearly seen from the GG/AG film (**Fig. 1**A), where the GG layer was homogeneous and smooth, while the AG layer was less uniform with some cracks. This phase separation between GG and AG layers was greatly attributed to the thermal irreversibility of GG and AG hydrogels, making them immiscible during the gelation process and thermal drying process. Meanwhile, there was no obvious gap at their interface, despite their distinct phase

separation. This could be due to their partial crosslinking through hydrogen bonding force based on their polysaccharide nature. This crosslinking at the interface was critical to developing a bilayer film. Otherwise, one monolayer film might be easy to peel off from the other monolayer film. The addition of AN improved the uniformity of AG layer.

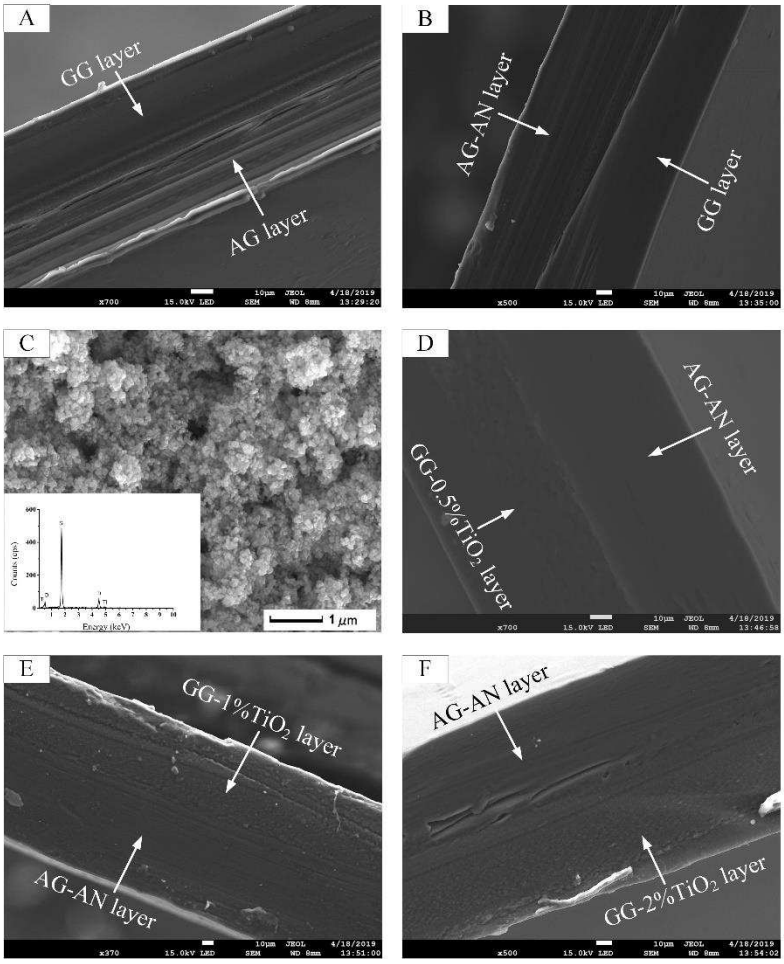

Fig. 1. The SEM images of cross section of (A) AG/GG film, (B) AG-AN/GG film, (D) AG-AN/GG-0.5%TiO_2 film, (E) AG-AN/GG-1%TiO_2 film and (F) AG-AN/GG-2%TiO_2 film, and (C) TiO_2 nanoparticles. Inset of (C) is the EDS spectrum of TiO_2 nanoparticles. The acceleration voltage was 15.0 KV.

It can be seen from **Fig. 1**B that the AG-AN layer was more compact and dense than the pure AG layer (**Fig. 1**A). The morphology of TiO_2 nanoparticles was shown in **Fig. 1**C. Most of the nanoparticles were sheet shapes and agglomerated to clusters, and the EDS spectrum (inset) verified the TiO_2 constituent. The TiO_2 nanoparticles could be observed from in the GG matrix of the AG-AN/GG-0.5%TiO_2 (**Fig. 1**D), AG-AN/GG-1%TiO_2 (**Fig. 1**E) and AG-AN/GG-2%TiO_2 (**Fig. 1**F) bilayer films. Meanwhile, as can be seen from the

Fig. 1F, no significant migration of TiO_2 nanoparticles from GG-TiO_2 layer to the AG-AN layer occurred even though the concentration of TiO_2 nanoparticles was 2% of the GG. Furthermore, the interface of the AG-AN layer and GG-TiO_2 layer remained well-crosslinked after the addition of TiO_2 nanoparticles. These results indicated that bilayer films, consisting of AG-AN and GG-TiO_2 layers, were successfully fabricated.

3.1.2. XRD spectra analysis

Fig. 2 shows the XRD spectra of TiO_2 nanoparticles and the films. TiO_2 nanoparticles exhibited strong diffraction peaks at 2θ = ~27.5°, 37.2° and 54.4°, verifying their rutile phase, which was in line with previous studies [40, 41]. The XRD pattern of AG/GG and AG-AN/GG film showed amorphous peaks at ~13.6° and ~19°, due to amorphous nature of agar (as a co-polymer of galactose and 3, 6-anhydro galactose) [42, 43]. A diffraction peak at 2θ = ~23° was the characteristic peak of gellan gum resulted from its double-helix crystal structures [16]. As for the AG-AN/GG-TiO_2 films, when TiO_2 concentration was relatively low (0.5 g/100 g GG), the crystalline structure of the nanoparticle was almost undetectable. This could be due to the coverage of GG molecular on the surface of the TiO_2. As the concentration of TiO_2 the GG layer increased to 2 g/100 g, the intensity of a characteristic peak (110) of rutile crystal phase increased, due to the self-assembled large TiO_2 agglomerates that recovered their crystallization ability. In addition, the diffraction intensity of GG (2θ = ~23°) presented a decreasing trend with the increase of TiO_2 content, indicating that the interaction between GG and TiO_2 decreased the crystallinity of GG. The possible interactions involved electrostatic attraction between negative-charge carboxylic groups from GG and positive-charge TiO^{4+}-water complex during the preparation of GG-TiO_2 solution [44].

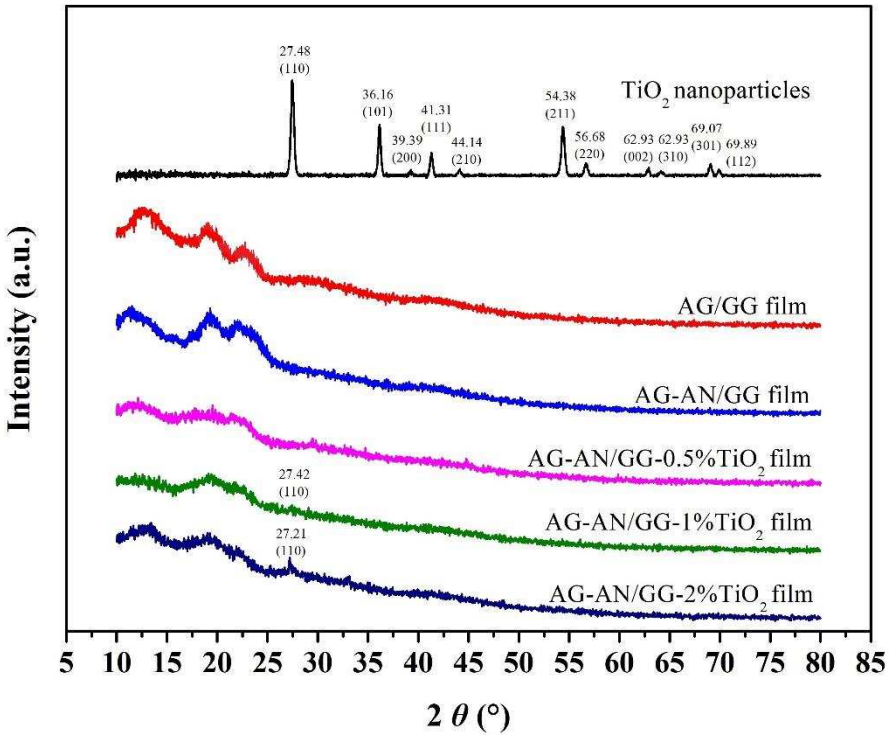

Fig. 2. The XRD spectra of TiO_2 nanoparticles and the bilayer films. The testing voltage and current were 40 kV and 40 mA, respectively.

3.1.3. Mechanical and barrier properties

The fundamental mechanical and barrier properties of the films, including TS, EB, WVP and OP, were shown in **Fig. 3**.

The AG/GG film showed the lowest TS (11.68 ± 1.72 MPa) (**Fig. 3**A) and highest EB value (36.82% ± 2.66%) (**Fig. 3**B). With the addition of AN to the AG layer, the TS value presented a weak increase, while the EB value slightly decreased. Incorporation of 1% TiO_2 into the AG-AN/GG film caused a significant increase of TS value (18.01 ± 2.36 MPa) ($p < 0.05$), but the TS decreased again with further addition of TiO_2 up to 2% (**Fig. 3**A). Meanwhile, the EB value of the AG-AN/GG-TiO_2 films declined with the increase of TiO_2 content (**Fig. 3**B). These results indicated that the incorporation of TiO_2 caused a rigid film due to the reinforcing effect in the GG matrix. However, the reduced TS value in the presence of 2% TiO_2 could be due to the aggregation and nonhomogeneous dispersion of TiO_2 particles that broke the compactness of the film.

WVP determines the moisture transfer between the surrounding atmosphere and the food environment. The WVP of the AG-GG film was 3.54 ± 0.32 g/mm/m^2/kPa/h, which decreased slightly when AN was added to the AG layer (**Fig. 3**C). The water permeability of a film is largely dependent on its chemical structure, morphology, and hydrophilicity. The decline of WVP of AG-GG film with the addition of AN could be due to the hydrogen bond between the AG and AN, which reduced the available of AG to form hydrogen bond with water. The further addition of 1% TiO_2 to the AG-AN/GG film significantly improve the water barrier ability, as the WVP of AG-AN/GG-1%TiO_2 film was 2.93 ± 0.22 g/mm/m^2/kPa/h. This was probably due to the prolonged tortuous pathway of water vapor formed by the well-distributed water impermeable nanoparticles [45]. Similar results were also found in chitosan-TiO_2 blend films [46] and wheat glute-nanocellulose-TiO_2 blend films [47]. The slight increase of WVP resulted from the addition of 2% TiO_2 to the AG-AN/GG film may also be due to the aggregation of TiO_2 that enlarge the crack between the crystals of GG. However, this increment was not significant ($P > 0.05$).

The oxygen barrier ability of the packaging films has great effect on the shelf life of packaged foods. The AG/GG film showed the highest OP value (40.80 ± 2.36 cm^3 μm/m^2/d/kPa) (**Fig. 3**D), which was comparable to polyvinyl chloride films (20-80 cm^3 μm/m^2/d/kPa). A significant decrease of OP value was observed when AG were incorporated into the AG/GG film. The oxygen barrier ability of the AG-AN/GG films were also notably improved by TiO_2. The OP value of the AG-AN/GG-2%TiO_2 film was 21.17 ± 1.55 cm^3 μm/m^2/d/kPa, which was nearly a half of the OP value of AG-AN/GG film. The remarkable enhancement of oxygen barrier ability of AG-AN/GG film induced by TiO_2 was due to the high aspect ratio of TiO_2 nanoparticles and their distribution throughout the film matrix. Incorporation of TiO_2 nanoparticles retarded the chain mobility via interfacial adhesion between TiO_2 and GG matrix, which provided lower vacant-free volume for oxygen transport [43]. In addition, the enhanced oxygen barrier ability of the GG-TiO_2 layer may improve the stability of AG-AN layer by reducing the oxidization of AN.

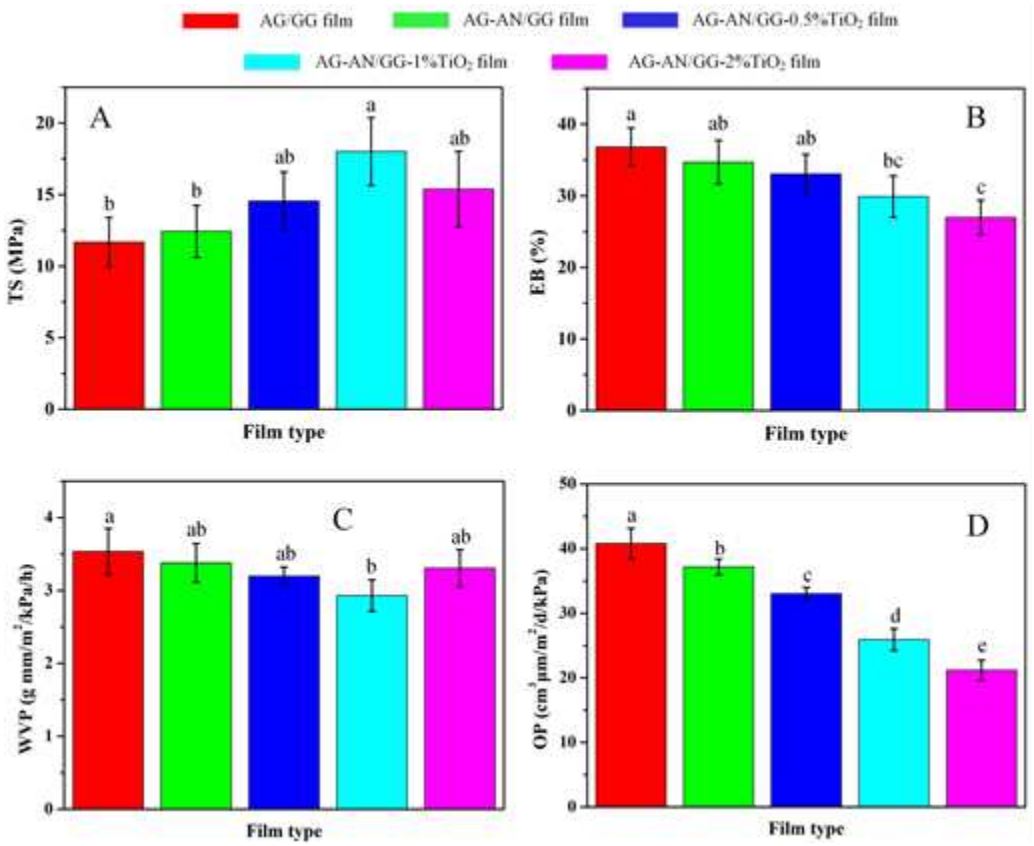

Fig. 3. The (A) TS, (B) EB, (C) WVP, (D) OP of the bilayer films.

3.2. Color response of AN to pH

The anthocyanins extracted from rose were employed as the pH-sensitive pigments to develop colorimetric films. Hence, the color response of the anthocyanins towards pH changes was investigated. The AN powder was added to pH buffer solutions prepared by using 0.2 M disodium hydrogen phosphate, 0.2 M citric acid and 0.2 M sodium hydroxide solutions with different proportions. **Fig. 4**A shows that anthocyanins solutions changed from red (pH 2-3) to colorless (pH 4-5), light purplish (pH 6-7), green (pH 8-11), and finally yellow (pH 12). Corresponding with the color changes in anthocyanins solutions, the maximum absorption peak (~520 nm) of the UV/Vis spectra decreased when the pH increased from 2 to 5, along with a red shift to ~550 nm (**Fig. 4**B). With the increase of pH from 6 ranging to 10, the maximum absorption peak showed a continuous red shift to nearly 595 nm (pH 10), accompanied by a rise of the maximum absorption peak. However, the maximum absorption peak showed a sharp drop when the pH was over 10. The absorbance ratio at 595 nm versus 520 nm (A_{595}/A_{520}) could indicate the increase of green color

intensity compared to red color [48]. As shown in **Fig. 4**C, the value of A_{595}/A_{520} firstly increased (pH 2-10) and then decreased (pH 10-12). Particularly, there was a good quadratic relationship between A_{595}/A_{520} and pH 2-10, with R^2 of 0.9935 of the calibration curve. This was different from purple sweet potato anthocyanins [48] and red radish anthocyanins solutions [34] that their absorbance ratios had good exponential relationships with pH values. The color changes of AN extracted from rose indicated that it could be a good candidate to develop a pH-sensitive colorimetric sensor.

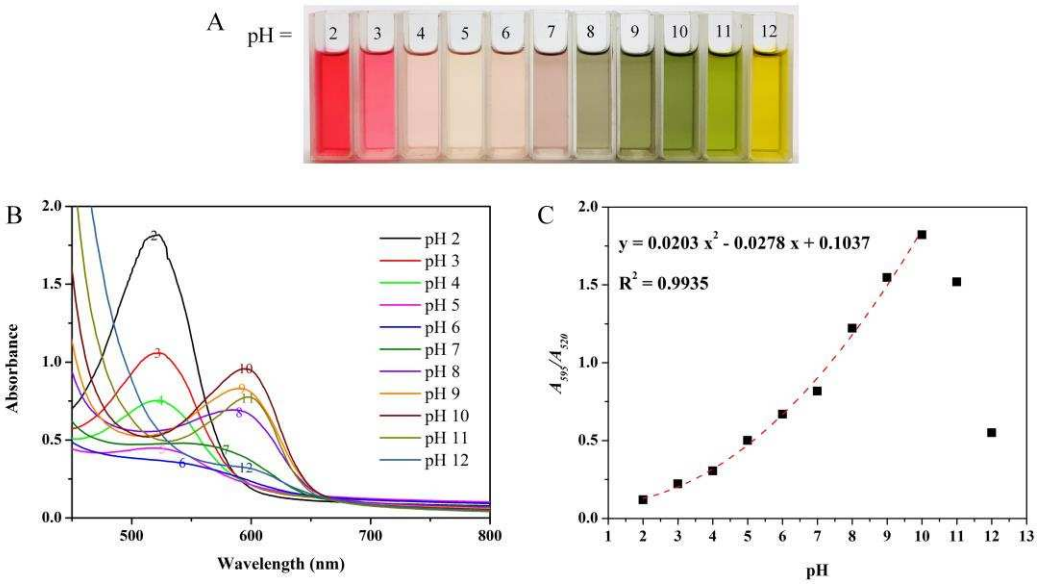

Fig. 4. The (A) color and (B) UV-Vis spectra of the rose anthocyanins solution under pH 2-12, and (C) the change of A_{595}/A_{520} of the rose anthocyanins solution with the increase of pH.

3.3. Color stability of the films under visible and UV light

The illumination stability of the films is important for practical application. In this study, the color stability of films exposed to visible light and UV light was tested, respectively.

The visible light was generated from a white fluorescent lamp (~ 400-760 nm). The colors of the films after a period of storage were shown in **Fig. 5**A. The AG/GG film showed a transparent and very pale yellow color due to the presence of agar. After stored under visible light at 25 °C for 21 days, its color was still well-maintained. The incorporation of AN endowed the AG/GG film a rose red color. All of the colorimetric films presented slight color changes after 21 days of storage. Especially for AG-AN/GG film, its color changed from rose red to purple red. The relative color change (S) was used

to quantify the color change of the films. A lower S value implied a superior color stability. As shown in **Fig. 5**B, the S value of AG/GG film kept nearly constant (< 1%), indicating its good color stability. In contrast, all the colorimetric films showed increasing S values with radiation time and the S values decreased with the increase of TiO_2 concentration. This improved color stability could be due to the physical light barrier ability (**Fig. S1**) and oxygen barrier ability (**Fig. 3**D) of TiO_2 that reduced the degradation of AN.

Generally, the UV of solar spectrum (100-400 nm) consists of the three ranges: UVA (400-315 nm), UVB (315-280 nm), and UVC (280-100 nm). In this study, the effect of UVA on the stability of the films was studied, because almost all of the UVC range and much of the UVB range light are absorbed by the stratospheric ozone layer [49]. The color of the films after exposed to a UVA light (λ = 320-400 nm with λ_{max} = 350 nm) were shown in **Fig. 5**C. It can be seen that AG/GG was colorless and no obvious color changes occurred in the AG/GG film after 35 hours of radiation. For colorimetric films, their colors showed a trend to brownness after UV radiation, due to the degradation of AN. This was because AN had strong UV absorption ability, as shown in **Fig. S1**, where the AG-AN/GG film had extremely low transparency in the range of 200-380 nm, compared with the AG/GG film. Especially, the highest S value (14.0% at the 35^{th} hour) was obtained from the AG-AN/GG film (**Fig. 5**D), indicating that AG-AN/GG film was most vulnerable to UV light. The addition of TiO_2 improved the stability of the colorimetric films. At the 35^{th} hour, the S values of AG-AN/GG-0.5%TiO_2 film and AG-AN/GG-1%TiO_2 film were 13.2% and 11.5%, respectively. When the concentration of TiO_2 increased to 2 wt% of the AG, the S value of AG-AN/GG-2%TiO_2 film was merely 8.4%, which was nearly a half of the S value of AG-AN/GG film. This significant improvement of color stability of the colorimetric films compared with AG-AN/GG film was attributed to the great UV absorption capacity of TiO_2 nanoparticles, whose band gap energy is of the magnitude order of the UV radiation energy [50, 51]. The rutile TiO_2 nanoparticles could transform high-energy UV light to less harmful heat or fluorescence [35]. In addition, TiO_2 nanoparticles have high chemical and thermal stability, and therefore they should be a promising UV blocking agent to protect anthocyanins from degradation.

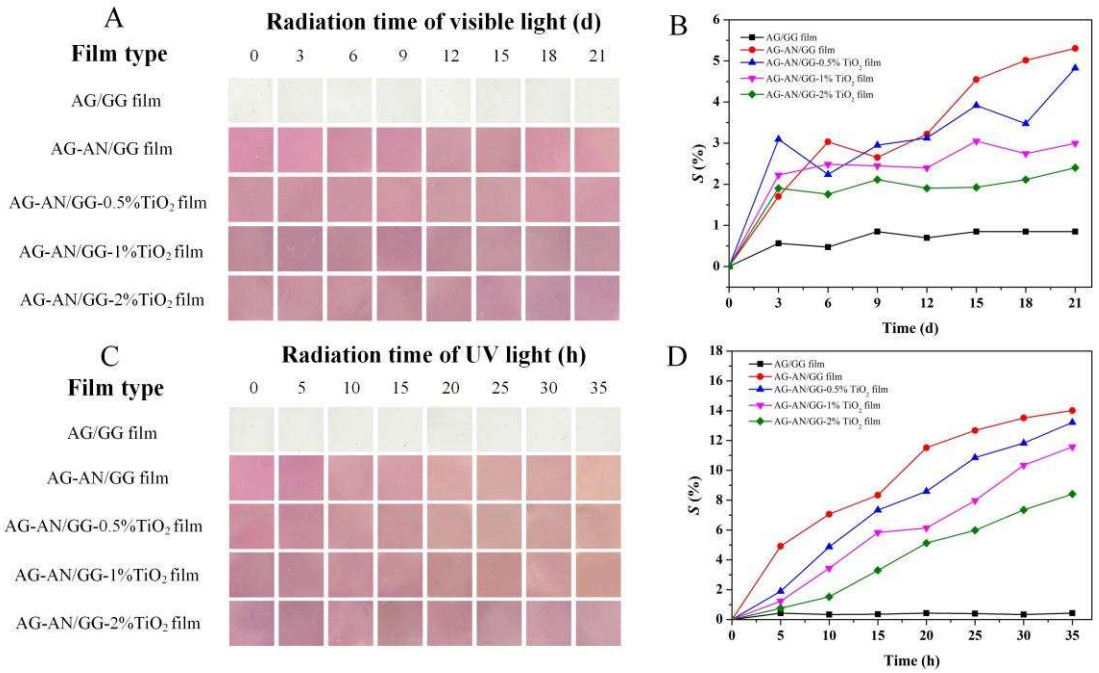

Fig. 5. The color changes of the bilayer films under (A) visible and (C) UV light, and the corresponding S values of the films under (B) visible and (D) UV light.

3.4. Electrochemical writing on bilayer films

The electrochemical writing is based on the color changes of anthocyanins induced by hydrogen ions and hydroxyl ions generated from water electrolytic reactions [32]. Hence, a hydrogel containing high water content is needed to be firstly fabricated. In this work, the AG-AN and GG-TiO_2 hydrogels were obtained due to the good gel-forming ability of AG and GG, respectively. In previous studies, the electrochemical writing was conducted on anthocyanins-containing monolayer hydrogels [32, 34]. Herein, the use of a bilayer hydrogel instead of a monolayer hydrogel in this work for electrochemical writing could make a better performance. As shown in **Scheme 2**, there are two ways for electrochemical writing on monolayer hydrogels. The first way is shown in **Scheme 2**A, the monolayer hydrogel is put on the Pt plate, and its upper surface is connected with the Pt needle. The Pt needle and Pt plate are respectively connected with the anode and cathode of the electrochemical workstation. Under a constant current (I), a localized low pH condition is generated around the Pt needle due to the anodic water electrolysis reaction (eq 11) so that anthocyanins turns to acid color (rose red). On the contrary, a localized high pH condition is generated around the Pt plate due to the anodic water electrolysis reaction (eq 12), and

therefore anthocyanins turns to basic color (yellow). In this way, the voltage (U) between the Pt needle and Pt plate is constant no matter where the Pt needle is located on the surface of the hydrogel. This is because the U is proportional to the resistance (R_e), while R_e is proportional to the perpendicular distance between the Pt needle and Pt plate, namely the thickness (d_1) of the hydrogel. However, the color change (yellow) of the entire lower surface of the hydrogel connected with the Pt plate is not favorable for its further use. The second way for electrochemical writing on monolayer hydrogels is that Pt plate is put to the side surface of the hydrogel, as shown in **Scheme 2**B. However, the U value between the Pt needle and Pt plate would exceed the measurement range of the electrochemical workstation, when the distance (d_2) between the Pt needle and Pt plate is overlarge. Hence, a bilayer hydrogel can be used to prevent the color changes of the hydrogel connected with the Pt plate and simultaneously make the voltage between the Pt needle and Pt plate constant. As shown in **Scheme 2**C, the AG-AN and GG-TiO_2 layer were connected with the Pt needle and Pt plate, respectively. In this way, the water electrolysis reaction round the Pt plate could not change the color of GG-TiO_2 hydrogel without anthocyanins. Meanwhile, the U value between the Pt needle and Pt plate is constant due to the constant distance (d_3) between the Pt needle and Pt plate.

$$2H_2O - 4e^- = 4H^+ + O_2 \uparrow \quad (11)$$

$$4H_2O + 4e^- = 4OH^- + 2H_2 \uparrow \quad (12)$$

The electrochemical writing patterns could be well preserved by immediately drying the hydrogels to films. By adjusting the magnitude and direction of the current, multicolor patterns, including English letters (**Fig. 6**A and **6**C), Chinese characters (**Fig. 6**B) and a geometrical shape (**Fig. 6**D), were successfully written on the colorimetric films. Hence, the bilayer films could be a good alternative for electrochemical writing.

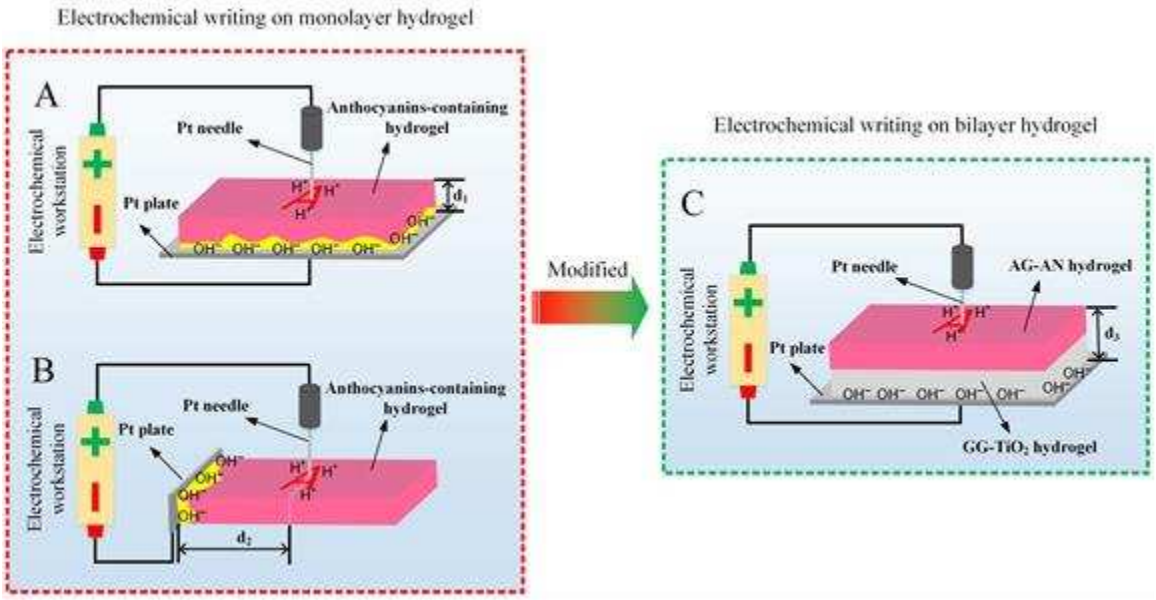

Scheme 2. The principle of electrochemical writing on monolayer and bilayer colorimetric films.

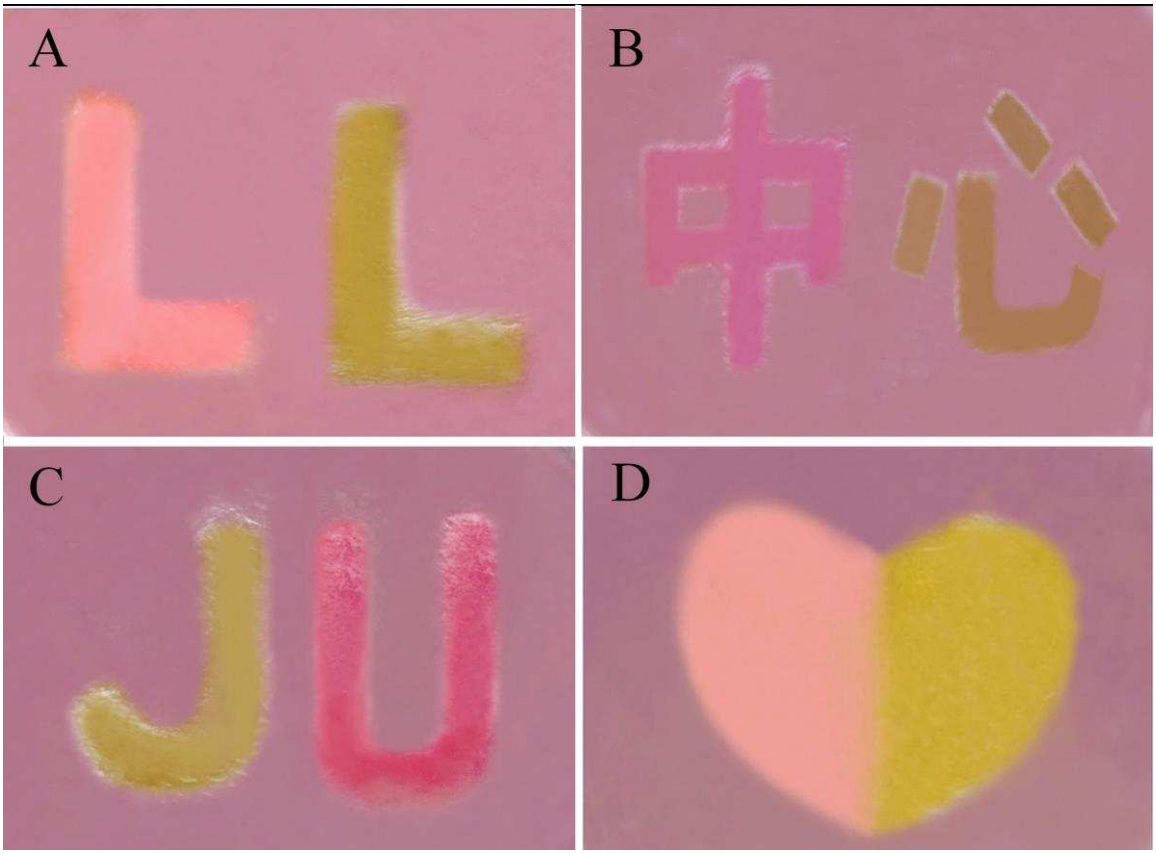

Fig. 6. The electrochemical writing patterns on (A) AG-AN/GG film, (B) AG-AN/GG-0.5%TiO_2 film, (C) AG-AN/GG-1%TiO_2 film and (D) AG-AN/GG-2%TiO_2 film.

3.5. Spectrum and color response to TMA

During meat spoilage, a mixture of ammonia, dimethylamine (DMA), trimethylamine (TMA), and other monoamines and polyamines can be generated via the metabolic breakdown of amino acids [52]. **Fig. S2** shows the images of the AG-AN/GG-2%TiO_2 film after being exposed to ammonia and three monoamines. The film turned to green in different degrees, indicating its sensing ability to volatile amines. The sensing principle is that the nitrogen-containing gases can combine with the water in the film and hydrolyze to generate hydroxyl ions, as shown in eq 13, and then hydroxyl ions can induce the color change of AN, as shown in eq 14, where the cyanidin changed from (1) flavylium ion to (2) anhydrobase, and then anhydrobase anion in the presence of hydroxyl ions.

$$R_3\text{-}N + H_2O \rightleftharpoons R_3\text{-}NH^+ + OH^- \quad (13)$$

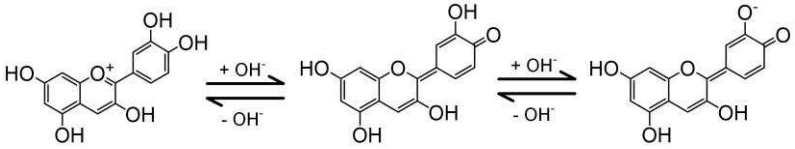

1 2 3 (14)

To simplify the experiment, TMA, a typical volatile monoamine, was selected as the representative gas to exam the sensitivity of the colorimetric films towards volatile amines. The color changes of colorimetric films towards TMA were shown in **Fig. 7**A. All the colorimetric films changed from rose red to green and final yellow color, when the TMA concentration gradually increased to 0.405 mM. The corresponding S values of the films also increased when the TMA concentration was up to 0.330 mM (**Fig. 7**B). Particularly, the films with different content of TiO_2 showed near S values, indicating that the presence of TiO_2 had no detrimental impact on the sensing ability of the film.

Furthermore, the sensitivity of AG-AN/GG-2%TiO_2 film to TMA was determined by using its UV-Vis spectra. As shown in **Fig. 7**C, the maximum absorption peak of AG-AN/GG-2%TiO_2 film decreased at 540 nm, but increased at 595 nm, when the concentration of TMA increased from 0 to 0.330 mM, which was in line with the spectrum change of AN solution with the increase of pH (**Fig. 4**B). Similarly, the absorbance ratio at 595 nm versus 540 nm (A_{595}/A_{540}) of AG-AN/GG-2%TiO_2 film progressively rose with

the increase of TMA concentration in the range of 0-0.330 mM, while declined when TMA concentration was as high as 0.405 mM (**Fig. 7**D). The A_{595}/A_{540} value presented a good linear relationship with TMA concentration in the range of 0-0.330 mM, with R^2 of 0.9881 of the calibration curve. Accordingly, the limit of detection (LOD) of AG-AN/GG-2%TiO_2 film to TMA was determined to be 0.018 mM, by using eq. 15:

$$\mathrm{LOD} = \frac{3K}{N} \tag{15}$$

Where K is the standard deviation of blank measurements and N is slope of the calibration curve.

In addition, the sensing ability of the film to TMA was largely associated with the relative humidity of test chamber. As shown in **Fig. S3**, at a constant TMA concentration (0.255 mM), the AG-AN/GG-2%TiO_2 film remained a red color under 30% relative humidity, while turned to green and then yellow under 75% and 90% relative humidity, respective. This indicated that a higher relative humidity contributed to generate more hydroxyl ions on the surface of the film. Similar results were also observed in curcumin-based films [26].

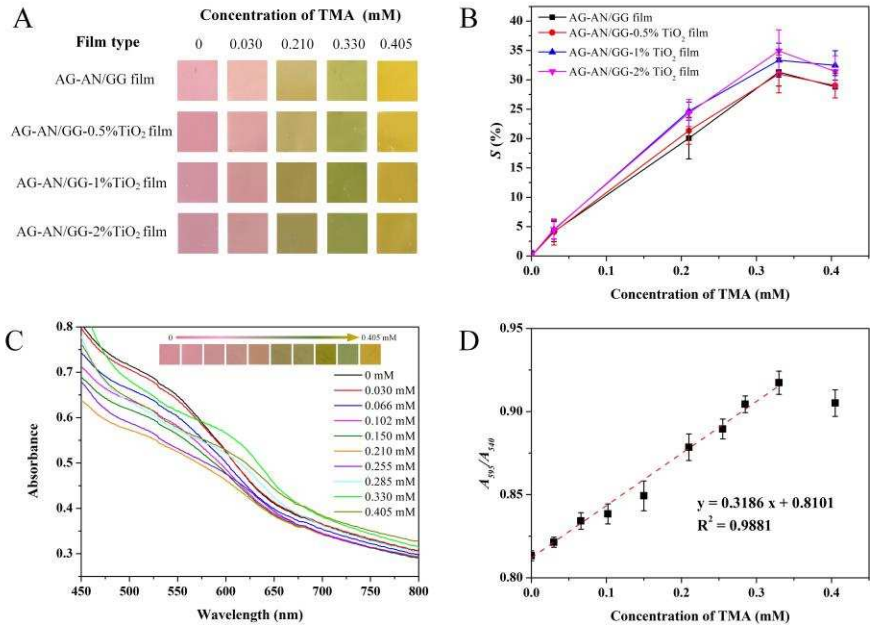

Fig. 7. The (A) colors and (B) S values of the colorimetric films in response to TMA at different concentrations; (C) UV-Vis spectra and colors (inset) of AG-AN/GG-2%TiO_2 film in response to TMA at 0-0.405 mM, and (D) the corresponding changes of A_{595}/A_{540} values of the AG-AN/GG-2%TiO_2 film with the concentration of TMA. The relative humidity and temperature of the testing chamber containing TMA were 75% and 25 ℃, respectively.

3.6. Application of films in monitoring meat spoilage

To test the feasibility of the bilayer film in monitoring meat spoilage, two square AG-AN/GG-2%TiO_2 films were fixed on the lid of a sealed PET box. As shown in **Fig. S4**, one film, expressed as film 1, was fixed on the external surface of the PET lid to cover the hole (15 mm length), while the other film, expressed as film 2, was directly adhered onto the internal surface of the PET lid.

It can be seen that film 1, as a water permeable window, showed visible color changes from rose red to light green, along with the cold storage (4 °C) of pork (**Fig. 8**A) and silver carp (**Fig. 8**B). By contrast, film 2, which was put inside of the sealed PET box, suffered from severe AN leaching, after absorbing a large amount of water vapor volatilized from the fresh meat samples. However, the AN leaching was not expected or controllable in this case. Hence, in this study, the film 1 was regarded as the meat spoilage indicator for further analysis.

The spoilage degree of the meats was evaluated by their TVB-N content. As shown in **Fig. 8**C and **8**D, the TVB-N values of the pork and silver samples respectively increased from 7.54 to 23.78 mg/ 100 g, and from 8.23 to 33.25 mg/ 100 g, after a 14-day storage. Meanwhile, the color changes of the AG-AN/GG-2%TiO_2 film could be quantitatively described by the rate of G value to the sum of R, G and B value, namely G/(R+G+B). It increased from 31.45% to 33.39% for pork, and increased from 32.26% to 34.10% for silver carp samples, respectively.

According to Chinese standard GB 2707-2016, the rejection limit of TVB-N level for fresh pork is 15 mg/100 g. In this study, the TVB-N value of pork increased to 15 mg/100 g at nearly 8 d, when the G/(R+G+B) value of the film was 32.55% (**Fig. 8**C). This indicated that if the G/(R+G+B) value was > 32.55%, then the pork sample should not be consumed. Similarly, according to Chinese standard GB 2733-2015, the rejection limit of TVB-N level for fresh silver carp is 20 mg/100 g. The TVB-N value of silver carp increased to 20 mg/100 g at nearly 8.5 d, when the G/(R+G+B) value of the film was 33.05 % (**Fig. 8**D). This implied that if the G/(R+G+B) value was > 33.05%, the silver carp sample should not be consumed.

Simultaneously, the color of the electrochemical patterns (yellow color) on the film 1 did not obviously changed, indicating its color stability on the film. Hence, the AG-AN/GG-2%TiO_2 films with the electrochemical patterns, which was worked as a colorimetric gas sensor, could be used to visually monitor the pork and silver carp spoilage.

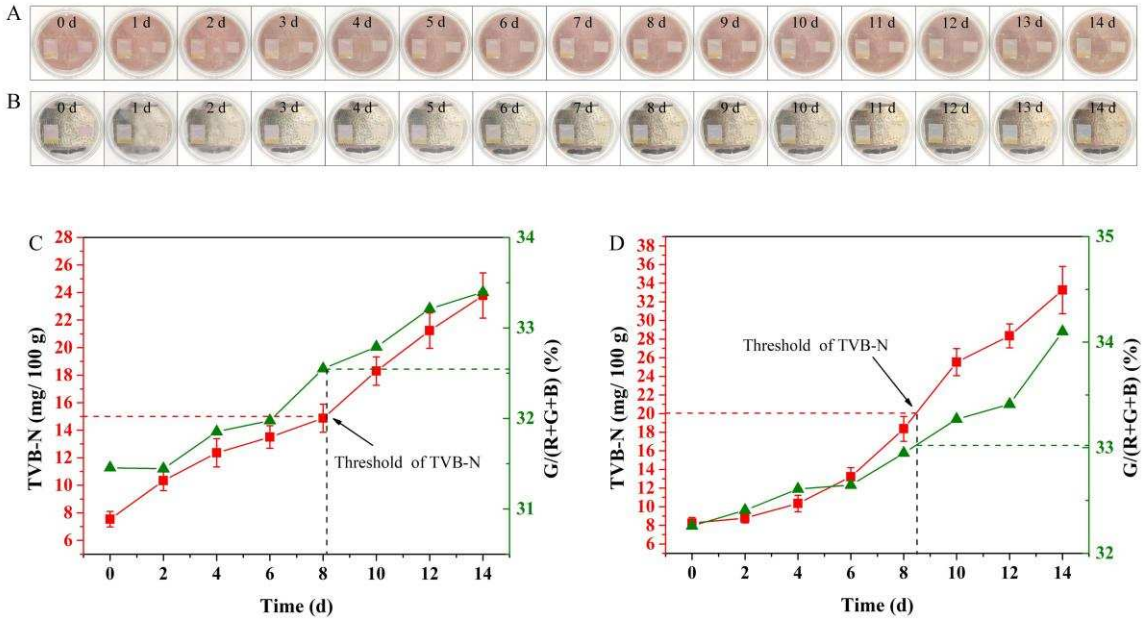

Fig. 8. The images of (A) pork and (B) silver carp, and the relation between TVB-N contents and G/(R+G+B) (%) values of AG-AN/GG-2%TiO_2 film in terms of (C) pork and (D) silver carp sample, during storage at 4 ℃.

3.7. Safety and cost of the films

The bilayer AG-AN/GG-TiO_2 films are safe and cost-effective. Anthocyanins and agar are well-known natural edible pigments and polysaccharide, respectively. GG is also an edible polysaccharide and has received both U.S. FDA and EU (E418) approval for application in a variety of foods [53]. Meanwhile, TiO_2 is included in the list of approved additives for food contact materials, according to the Commission Regulation (EU) No. 10/2011 on plastics and articles intended to come into contact with foods [54]. For one thousand AG-AN/GG-2%TiO_2 films (diameters 53 mm), the total cost of the materials is merely $ 17.15 (**Table S1**). Therefore, the colorimetric film is not only a safe meat spoilage indicator, but an economical sensor for intelligent food packaging.

4. Conclusions

Bilayer colorimetric films, including AG/GG, AG-AN/GG, AG-AN/GG-0.5%TiO_2, AG-AN/GG-1%TiO_2 and AG-AN/GG-2%TiO_2 film, were successfully developed through a two-step casting technique. SEM images and XRD spectra verified the successful fabrication of the bilayer films. The incorporation of TiO_2 up to 1 g/100 g of GG significantly improved the tensile strength, water barrier ability and oxygen barrier ability of the AG-AN/GG film, while the flexibility of the AG-AN/GG-TiO_2 films decreased with the increase of TiO_2 content up to 2 g/100 g of GG. The color stability of the colorimetric films under visible and UV light was enhanced with the increase of TiO_2 content. The presence of TiO_2 did not hinder the TMA-sensing ability of AN, and the LOD of AG-AN/GG-2%TiO_2 film to TMA was 0.018 mM. The AG-AN/GG-2%TiO_2 film exhibited visible color changes along with the storage of pork and silver carp at 4 °C, and it was safe and cost-effective. Hence, the bilayer films should have good potential for practical application in intelligent food packaging.

Acknowledgments

The authors gratefully acknowledge the financial support provided by the National Key Research and Development Program of China (2016YFD0401104, 2017YFC1600805, 2018YFD0400803, 2017YFC1600806, 2017YFD0400102-3, 2018YFD0701001), the National Natural Science Foundation of China (31671844, 31601543, 31801631, 31772073), the Natural Science Foundation of Jiangsu Province (BK20160506, BE2016306), the Postgraduate Research & Practice Innovation Program of Jiangsu Province (KYCX17_1798), Priority Academic Program Development of Jiangsu Higher Education Institutions (PAPD) and the Project of Faculty of Agricultural Equipment of Jiangsu University.

Declarations of interest

None.

Reference

[1] G.J. Nychas, P.N. Skandamis, C.C. Tassou, K.P. Koutsoumanis, Meat spoilage during distribution, Meat Sci. 78(2008) 77-89.

[2] R. Jia, W. Tian, H. Bai, J. Zhang, S. Wang, J. Zhang, Amine-responsive cellulose-based ratiometric fluorescent materials for real-time and visual detection of shrimp and crab freshness, Nat. Commun. 10(2019) 795.

[3] A. Pacquit, J. Frisby, D. Diamond, K.T. Lau, A. Farrell, B. Quilty, et al., Development of a smart packaging for the monitoring of fish spoilage, Food Chem. 102(2007) 466-70.

[4] C. Zhang, A.X. Yin, R. Jiang, J. Rong, L. Dong, T. Zhao, et al., Time-temperature indicator for perishable products based on kinetically programmable Ag overgrowth on Au nanorods, Acs Nano, 7(2013) 4561-8.

[5] X. Zhai, Z. Li, J. Shi, X. Huang, Z. Sun, D. Zhang, et al., A colorimetric hydrogen sulfide sensor based on gellan gum-silver nanoparticles bionanocomposite for monitoring of meat spoilage in intelligent packaging, Food Chem. 290(2019) 135-43.

[6] T. Lin, Y. Wu, Z. Li, Z. Song, L. Guo, F. Fu, Visual monitoring of food spoilage based on hydrolysis-induced silver Metallization of Au Nanorods, Anal. Chem. 88(2016) 11022-7.

[7] F. Saliu, R. Della Pergola, Carbon dioxide colorimetric indicators for food packaging application: applicability of anthocyanin and poly-lysine mixtures, Sens. Actuators B 258(2018) 1117-24.

[8] Y.C. Wang, L. Lu, S. Gunasekaran, Biopolymer/gold nanoparticles composite plasmonic thermal history indicator to monitor quality and safety of perishable bioproducts, Biosens. Bioelectron. 92(2017) 109-16.

[9] H. Xiao-wei, Z. Xiao-bo, S. Ji-yong, L. Zhi-hua, Z. Jie-wen, Colorimetric sensor arrays based on chemo-responsive dyes for food odor visualization, Trends Food Sci Technol. 81(2018) 90-107.

[10] B. Kuswandi, Jayus, A. Restyana, A. Abdullah, L.Y. Heng, M. Ahmad, A novel colorimetric food package label for fish spoilage based on polyaniline film, Food Control 25(2012) 184-9.

[11] C. Rukchon, A. Nopwinyuwong, S. Trevanich, T. Jinkarn, P. Suppakul, Development of a food spoilage indicator for monitoring freshness of skinless chicken breast, Talanta 130(2014) 547-54.

[12] X. Zhang, S. Lu, X. Chen, A visual pH sensing film using natural dyes from Bauhinia blakeana Dunn, Sens. Actuators B 198(2014) 268-73.

[13] C.L. Luchese, V.F. Abdalla, J.C. Spada, I.C. Tessaro, Evaluation of blueberry residue incorporated cassava starch film as pH indicator in different simulants and foodstuffs, Food Hydrocoll. 82(2018) 209-18.

[14] V.A. Pereira, I.N.Q. de Arruda, R. Stefani, Active chitosan/PVA films with anthocyanins from Brassica oleraceae (Red Cabbage) as time–temperature indicators for application in intelligent food packaging, Food Hydrocoll. 43(2015) 180-8.

[15] M.C. Silva-Pereira, J.A. Teixeira, V.A. Pereira-Júnior, R. Stefani, Chitosan/corn starch blend films with extract from Brassica oleraceae (red cabbage) as a visual indicator of fish deterioration, LWT - Food Sci. Technol. 61(2015) 258-62.

[16] Y.-C. Wei, C.-H. Cheng, Y.-C. Ho, M.-L. Tsai, F.-L. Mi, Active gellan gum/purple sweet potato composite films capable of monitoring pH variations, Food Hydrocoll. 69(2017) 491-502.

[17] X. Zhai, J. Shi, X. Zou, S. Wang, C. Jiang, J. Zhang, et al., Novel colorimetric films based on starch/polyvinyl alcohol incorporated with roselle anthocyanins for fish freshness monitoring, Food Hydrocoll. 69(2017) 308-17.

[18] Q. Ma, L. Wang, Preparation of a visual pH-sensing film based on tara gum incorporating cellulose and extracts from grape skins, Sens. Actuators B 235(2016) 401-7.

[19] Q. Ma, Y. Ren, Z. Gu, L. Wang, Developing an intelligent film containing Vitis amurensis husk extracts: The effects of pH value of the film-forming solution, J. Cleaner Prod. 166(2017) 851-9.
[20] S. Kang, H. Wang, M. Guo, L. Zhang, M. Chen, S. Jiang, et al., Ethylene-vinyl alcohol copolymer/montmorillonite multilayer barrier film coated with mulberry anthocyanin for freshness monitoring, J. Agric. Food Chem. 66(2018) 13268-13276.
[21] P. Ezati, H. Tajik, M. Moradi, Fabrication and characterization of alizarin colorimetric indicator based on cellulose-chitosan to monitor the freshness of minced beef, Sens. Actuators B 285(2019) 519-28.
[22] J. Zhang, X. Zou, X. Zhai, X. Huang, C. Jiang, M. Holmes, Preparation of an intelligent pH film based on biodegradable polymers and roselle anthocyanins for monitoring pork freshness, Food Chem. 272(2019) 306-12.
[23] I. Dudnyk, E.-R. Janeček, J. Vaucher-Joset, F. Stellacci, Edible sensors for meat and seafood freshness, Sen. Actuators B 259(2018) 1108-12.
[24] H. Yong, X. Wang, R. Bai, Z. Miao, X. Zhang, J. Liu, Development of antioxidant and intelligent pH-sensing packaging films by incorporating purple-fleshed sweet potato extract into chitosan matrix, Food Hydrocoll. 90(2019) 216-24.
[25] B. Kuswandi, Jayus, T.S. Larasati, A. Abdullah, L.Y. Heng, Real-time monitoring of shrimp Spoilage Using on-package sticker sensor based on natural dye of curcumin, Food Anal. Method. 5(2011) 881-9.
[26] Q. Ma, L. Du, L. Wang, Tara gum/polyvinyl alcohol-based colorimetric NH_3 indicator films incorporating curcumin for intelligent packaging, Sens. Actuators B 244(2017) 759-66.
[27] J. Liu, H. Wang, P. Wang, M. Guo, S. Jiang, X. Li, et al., Films based on κ-carrageenan incorporated with curcumin for freshness monitoring, Food Hydrocoll. 83(2018) 134-142.
[28] Y.S. Musso, P.R. Salgado, A.N. Mauri, Smart edible films based on gelatin and curcumin, Food Hydrocoll. 66(2017) 8-15.
[29] A. Castañeda-Ovando, M.d.L. Pacheco-Hernández, M.E. Páez-Hernández, J.A. Rodríguez, C.A. Galán-Vidal, Chemical studies of anthocyanins: A review, Food Chem. 113(2009) 859-71.
[30] F. Weber, K. Boch, A. Schieber, Influence of copigmentation on the stability of spray dried anthocyanins from blackberry, LWT - Food Sci. Technol. 75(2017) 72-7.
[31] A. Bąkowska, A.Z. Kucharska, J. Oszmiański, The effects of heating, UV irradiation, and storage on stability of the anthocyanin–polyphenol copigment complex, Food Chem. 81(2003) 349-55.
[32] S. Wu, W. Wang, K. Yan, F. Ding, X. Shi, H. Deng, et al., Electrochemical writing on edible polysaccharide films for intelligent food packaging, Carbohydr. Polym. 186(2018) 236-42.
[33] K. Yan, Y. Xiong, S. Wu, W.E. Bentley, H. Deng, Y. Du, et al., Electro-molecular assembly: electrical writing of information into an erasable polysaccharide medium, ACS Appl. Mat. Interfaces 8(2016) 19780.
[34] X. Zhai, Z. Li, J. Zhang, J. Shi, X. Zou, X. Huang, et al., Natural biomaterial-based edible and ph-sensitive films combined with electrochemical writing for intelligent food packaging, J. Agric. Food Chem. 66(2018) 12836-46.
[35] C. Mana, Y. Liu, W. Wang, W. Ren, J. Long, F. Reisdorffer, et al., Poly (lactic acid)/titanium dioxide composites: preparation and performance under ultraviolet irradiation, Polym. Degrad. Stab. 97(2012) 856-62.
[36] G. De Filpo, A.M. Palermo, R. Munno, L. Molinaro, P. Formoso, F.P. Nicoletta, Gellan gum/titanium dioxide nanoparticle hybrid hydrogels for the cleaning and disinfection of parchment, Int. Biodeterior. Biodegrad. 103(2015) 51-8.
[37] Z. Wang, Y. Li, L. Chen, X. Xin, Q. Yuan, A study of controlled uptake and release of anthocyanins by oxidized starch microgels, J. Agric. Food Chem. 61(2013) 5880-7.

[38] H. Xiaowei, Z. Xiaobo, Z. Jiewen, S. Jiyong, L. Zhihua, S. Tingting, Monitoring the biogenic amines in Chinese traditional salted pork in jelly (Yao-meat) by colorimetric sensor array based on nine natural pigments, Int. J. Food Sci. Tech. 50(2015) 203-9.
[39] J. Cai, Q. Chen, X. Wan, J. Zhao, Determination of total volatile basic nitrogen (TVB-N) content and Warner-Bratzler shear force (WBSF) in pork using Fourier transform near infrared (FT-NIR) spectroscopy, Food Chem. 126(2011) 1354-60.
[40] Y.S. Hu, L. Kienle, Y.G. Guo, J. Maier, High lithium electroactivity of nanometer-sized rutile TiO_2, Adv. Mater. 18(2006) 1421-6.
[41] K. Thamaphat, P. Limsuwan, B. Ngotawornchai, Phase characterization of TiO_2 powder by XRD and TEM, Kasetsart J. (Nat. Sci.) 42(2008) 357-61.
[42] M. Atef, M. Rezaei, R. Behrooz, Preparation and characterization agar-based nanocomposite film reinforced by nanocrystalline cellulose, Int. J. Biol. Macromol. 70(2014) 537-44.
[43] Y.A. Arfat, J. Ahmed, H. Jacob, Preparation and characterization of agar-based nanocomposite films reinforced with bimetallic (Ag-Cu) alloy nanoparticles, Carbohydr. Polym. 155(2017) 382-90.
[44] J.J. Zhou, S.Y. Wang, S. Gunasekaran, Preparation and characterization of whey protein film incorporated with TiO_2 nanoparticles, J. Food Sci. 74(2010) N50-N6.
[45] S. Roy, J.-W. Rhim, L. Jaiswal, Bioactive agar-based functional composite film incorporated with copper sulfide nanoparticles, Food Hydrocoll. 93(2019) 156-66.
[46] U. Siripatrawan, P. Kaewklin, Fabrication and characterization of multifunctional active food packaging from chitosan-titanium dioxide nanocomposite as ethylene scavenging and antimicrobial film, Food Hydrocoll. 84(2018) 125-134.
[47] N.A. El-Wakil, E.A. Hassan, R.E. Abou-Zeid, A. Dufresne, Development of wheat gluten/nanocellulose/titanium dioxide nanocomposites for active food packaging, Carbohydr. Polym. 124(2015) 337-46.
[48] I. Choi, J.Y. Lee, M. Lacroix, J. Han, Intelligent pH indicator film composed of agar/potato starch and anthocyanin extracts from purple sweet potato, Food Chem. 218(2017) 122-8.
[49] T.M. Rünger, Solar Ultraviolet Light, in: M. Schwab (Ed.) Encyclopedia of Cancer, Springer Berlin Heidelberg, Berlin, Heidelberg, 2009, pp. 2774-8.
[50] L. Chuanan, W. Qing, S. Teng, Z. Da, W. Qingsheng, W. Qigang, Nanocomposite gels via in situ photoinitiation and disassembly of TiO_2-clay composites with polymers applied as UV protective films, ACS Appl. Mat. Interfaces 6(2014) 1356.
[51] L.C. Mohr, A.P. Capelezzo, C.R.D.M. Baretta, M.A.P.M. Martins, M.A. Fiori, J.M.M. Mello, Titanium dioxide nanoparticles applied as ultraviolet radiation blocker in the polylactic acid bidegradable polymer, Polym. Test. (2019) 105867.
[52] N. Wells, D. Yusufu, A. Mills, Colourimetric plastic film indicator for the detection of the volatile basic nitrogen compounds associated with fish spoilage, Talanta 194(2019) 830-6.
[53] C.J. Ferris, K.J. Gilmore, G.G. Wallace, M.I.H. Panhuis, Modified gellan gum hydrogels for tissue engineering applications, Soft Matter 9(2013) 3705-11.
[54] C. Garcia, G. Hwa Shin, J.T. Kim, Metal oxide-based nanocomposites in food packaging: applications, migration, and regulations, Trends Food Sci. Technol. 82(2018) 21-31.